Toward a High-Stability Coherent Population Trapping Cs Vapor-Cell Atomic Clock Using Autobalanced Ramsey Spectroscopy

Moustafa Abdel Hafiz,[1] Grégoire Coget,[1] Michael Petersen,[1] Cyrus Rocher,[1] Stéphane Guérandel,[2] Thomas Zanon-Willette,[3] Emeric de Clercq,[2] and Rodolphe Boudot[1]

[1]*FEMTO-ST, CNRS, UBFC, ENSMM, 26 rue de l'épitaphe 25030 Besançon, France*
[2]*LNE-SYRTE, Observatoire de Paris, Université PSL, CNRS, Sorbonne Université, 61 avenue de l'Observatoire, 75014 Paris, France*
[3]*Sorbonne Université, Observatoire de Paris, Université PSL, CNRS, LERMA, F-75005 Paris, France*

(Received 23 December 2017; revised manuscript received 15 March 2018; published 1 June 2018)

Vapor-cell atomic clocks are widely appreciated for their excellent short-term fractional frequency stability and their compactness. However, they are known to suffer on medium and long time scales from significant frequency instabilities, generally attributed to light-induced frequency-shift effects. In order to tackle this limitation, we investigate the application of the recently proposed autobalanced Ramsey (ABR) interrogation protocol onto a pulsed hot-vapor Cs vapor-cell clock based on coherent population trapping (CPT). We demonstrate that the ABR protocol, developed initially to probe the one-photon resonance of quantum optical clocks, can be successfully applied to a two-photon CPT resonance. The applied method, based on the alternation of two successive Ramsey-CPT sequences with unequal free-evolution times and the subsequent management of two interconnected phase and frequency servo loops, is found to allow a relevant reduction of the clock-frequency sensitivity to laser-power variations. This original ABR-CPT approach, combined with the implementation of advanced electronics laser-power stabilization systems, yields the demonstration of a CPT-based Cs vapor-cell clock with a short-term fractional frequency stability at the level of $3.1 \times 10^{-13}\tau^{-1/2}$, averaging down to the level of 6×10^{-15} at 2000-s integration time. These encouraging performances demonstrate that the use of the ABR interrogation protocol is a promising option towards the development of high-stability CPT-based frequency standards. Such clocks could be attractive candidates in numerous applications including next-generation satellite-based navigation systems, secure communications, instrumentation, or defense systems.

DOI: 10.1103/PhysRevApplied.9.064002

I. INTRODUCTION

High-performance compact microwave atomic clocks are attractive candidates in numerous applications since they can exhibit modest size, power consumption, cost, and excellent fractional frequency stability. Widely used ubiquitous devices are commercial Cs beam clocks [1,2] and Rb vapor-cell clocks [3,4]. These two types of clocks have known over the last decades a large success including their deployment in space applications [5,6]. Yet, multiple novel interrogation schemes and techniques are actively pursued and explored towards the development of next-generation high-performance compact vapor-cell clocks [7], targeting either reduced dimensions and power or improved frequency stability.

The use of coherent-population-trapping (CPT) spectroscopy [8,9], allowing the probing of a microwave clock transition frequency in an all-optical way, has turned out to be an elegant option for the development of high-performance compact atomic clocks. Vapor-cell CPT clocks have already demonstrated outstanding short-term instabilities at the level of a few $10^{-13}\tau^{-1/2}$ up to 100 s averaging time [10–13]. However, these clocks suffer in general on longer time scales from significant frequency drifts, preventing them to be fully competitive with best compact vapor-cell atomic clocks [14,15]. In the following, we will use the expression midterm for times between 100 and 10^4 s, and long term for times greater than 10^4 s.

A first important contribution to the clock mid- and long-term fractional frequency stability of CPT clocks is the buffer-gas-induced temperature-dependent frequency shift, usually measured in fractional value at the level of a few 10^{-10}/K [16–18]. Hopefully, this contribution can be significantly reduced by using a properly tuned buffer gas mixture [19,20], stabilizing finely the cell temperature below the mK level and adopting a well-designed alkali cell geometry to prevent any abnormally large temperature sensitivity [21].

A second major contribution to the mid- and long-term fractional frequency stability of CPT clocks is known to be light-induced frequency shifts, which depend on the laser power, the laser frequency, but also on the CPT sideband asymmetry through the microwave power of the signal that modulates the laser system [11–13,20,22]. These shifts are induced by conventional ac-Stark shifts caused by off-resonant interactions [23] or arise from both resonant optical transitions involved in the Λ scheme when incomplete dark states are created [24,25].

Most of the CPT clocks, including chip-scale atomic clocks [26,27], operate with the continuous Rabi interrogation scheme. The main drawbacks of CW-regime CPT clocks are to suffer from a significant CPT line-power broadening and more especially to exhibit a relevant dependence of the clock frequency to variations of the light field. Typical frequency sensitivities to laser-power and laser-frequency variations in CW-regime CPT clocks are measured to be in fractional value a few $10^{-12}/\mu$W and a few 10^{-12}/MHz, respectively [11,12]. Several methods have been reported in CW-regime CPT clocks to reduce the sensitivity of the clock frequency to light-field variations. This includes, for instance, the active stabilization of a specific *magic* microwave power [22,28–30], the adjustment of a specific cell temperature [31], or the fine-tuning of the laser temperature [28].

An alternative promising option is to use the Ramsey's method of separated oscillating fields [32], in which the single oscillatory field is replaced by a double microwave excitation pulse separated by a free-evolution time. The application of Ramsey spectroscopy with CPT has been reported on a sodium atomic beam [33] and later investigated in an important number of groups, especially in vapor-cell clock experiments [13,23,34–43]. The Ramsey-CPT method offers the main advantages to produce narrow-linewidth Ramsey-CPT fringes whose linewidth depends mainly on the free-evolution time, and more especially to induce resonant light shifts scaling inversely with the Ramsey period, as shown theoretically and recently experimentally with vapor-cell or cold-atom CPT experiments [13,44]. This key feature of the Ramsey-CPT method, combined with enhanced phase coherence of the Raman beam and use of an optimized CPT pumping scheme, has allowed recently the demonstration of a low-drift cold-atom CPT clock exhibiting an Allan deviation of $1.3 \times 10^{-11}\tau^{-1/2}$ averaging down to 2×10^{-13} after 40 000 s [45,46]. At the opposite, the use of Ramsey spectroscopy has not demonstrated so far an improvement in long-term clock stability over continuous interrogation in hot-vapor-cell CPT clocks [13,17].

Despite its great resolution, the original Ramsey method remains very sensitive to perturbations from the probe field itself. Over the last decade, impressive theoretical efforts have been pursued to propose robust interrogation protocols targeting to eliminate the contribution of the probing-field-induced clock-frequency shifts. In 2009, Taichenachev *et al.* proposed for optical clock transitions to extend Ramsey spectroscopy by applying a frequency step to the probing field, equal to the light shift, during the two Ramsey excitation pulses in order to compensate frequency shifts induced by the excitation itself [47]. This method has been improved by the so-called hyper-Ramsey spectroscopy technique [48], successfully demonstrated onto a Yb^+-ion optical clock experiment [49], later extended to the method of modified hyper-Ramsey spectroscopy [50] and to another variant proposed in Ref. [51]. In 2016, Yudin *et al.* adapted their synthetic frequency protocol, initially developed to suppress the blackbody radiation shift [52], to a universal interrogation protocol where an error signal is generated from sequences with different dark time intervals and allowing to reduce significantly imperfect correction of probe-induced frequency shifts even in the presence of decoherence due to the laser linewidth [53]. This method has been later extended in the general case where both decoherence and relaxation dissipation effects are present [54]. In this case, the error signal is calculated from the combination of several error signals generated from different generalized Hyper-Ramsey spectroscopy sequences.

More recently, an alternative interrogation protocol named autobalanced Ramsey (ABR) spectroscopy has been proposed [55]. This method is based on the combination of two successive Ramsey sequences with unequal free-evolution times, yielding the management of two interconnected phase and frequency servo loops. The first Ramsey cycle, with short free-evolution time, allows the extraction of an error signal used to apply a phase-step correction to the interrogation field between the Ramsey pulses. The second Ramsey cycle, with long free-evolution time, generates an error signal used to lock the probing-field mean frequency. The efficiency of this method has been experimentally demonstrated in an $^{171}Yb^+$ ion optical clock, yielding a final reduction by about 10^4 of the light-shift coefficient [55].

In this article, we demonstrate theoretically and experimentally the possible application of the ABR interrogation protocol to a CPT-based Cs vapor-cell atomic clock. Compared to the usual Ramsey-CPT regime, the ABR-CPT protocol is found to allow a relevant reduction of the clock-frequency dependence to laser-power variations. Additionally, a dedicated laser power servo operating in the pulsed regime and improved thermal isolation of the experiment have been implemented for improvement of the clock performances. The clock Allan deviation in the Ramsey-CPT regime is measured to be $1.4 \times 10^{-13}\tau^{-1/2}$ up to 200 s, degrading after to reach 10^{-13} at 10^4 s. In the ABR-CPT regime, the clock short-term frequency stability is degraded by a factor of 2 to $3.1 \times 10^{-13}\tau^{-1/2}$. At the opposite, the clock mid-term frequency stability is improved in the ABR-CPT regime, yielding the promising level of 6×10^{-15} at 2000 s integration time.

II. A SIMPLE MODEL FOR AUTOBALANCED RAMSEY WITH CPT

We present here a simple model based on materials from Refs. [56,57] in order to support the experimental demonstration reported in Sec. V of enhanced immunity to probing-field-induced frequency shifts using the autobalanced Ramsey-CPT (ABR-CPT) interrogation protocol. We suppose a basic three-level system excited by two coherent lasers where the first pulse is long enough to allow a complete atomic preparation into the dark-state superposition and a second delayed very short pulse to probe that superposition. The three-level system includes two ground-state hyperfine levels, labeled 1 and 2, and an excited level noted 3. The optical transitions are driven by Rabi frequencies $\Omega_{1,2}$, where subscripts 1,2 refer to the involved ground state. The spontaneous emission rates Γ_{31}, Γ_{32}, optical coherence relaxations $\gamma_{1,2}$ and a Raman decoherence γ_c are taken into account. We suppose in the adiabatic regime that the short probe pulse operation is well described by a stationary line shape with Raman-Ramsey CPT fringes including a phase-shift expression free from any time dependence as in Ref. [56].

For a free-evolution time T, the oscillating part of the Raman-Ramsey signal can be written as $\cos(\delta T - \Phi)$, with δ the Raman detuning (i.e., laser frequency difference minus ground-state hyperfine splitting), and Φ the accumulated effective phase including the light-induced frequency shifts during the optical pulses. In order to stabilize the frequency of a local oscillator (LO) on the hyperfine splitting frequency, a phase modulation $\pm\pi/2$ is applied between two sequential pulses. A dispersion-shape error signal is then obtained, scaling as $\sin(\delta T - \Phi)$, by differentiating two successive Ramsey signals. In usual Ramsey experiments, the probe frequency is locked with a detuning $\delta = \Phi/T$. The originality of the ABR technique [55] is the use of two alternate Ramsey sequences, one with a long free-evolution time T_1, the other with a shorter time T_2, and two interleaved servo loops. The error signal generated by the T_1 sequence is then used to lock the frequency at $\delta = 0$, while the error signal of the T_2 sequence allows correction of Φ with an additional phase step φ_c, such that $-\Phi + \varphi_c = 0$.

To demonstrate analytically the robustness of a phase-frequency stabilization on the unperturbed Raman clock transition by autobalanced Ramsey spectroscopy, we give the explicit form of the set of interleaved loop equations, expressed as follows:

$$\delta(\varphi_c) \circlearrowleft \begin{array}{c} \delta \mathrm{T}_1 - \Phi(\delta) + \varphi_c = 0 \\ \delta \mathrm{T}_2 - \Phi(\delta) + \varphi_c = 0 \end{array} \circlearrowright \varphi_c(\delta), \qquad (1)$$

where φ_c is applied before the second Ramsey-CPT pulse of each sequence. In our simplified model the probe-induced shifts η_1, η_2 are introduced in the optical detunings as follows: $\Delta_1 = \eta_1 + \delta/2$ and $\Delta_2 = \eta_2 - \delta/2$, where we assume η_1, η_2 proportional to Ω_1^2, Ω_2^2, respectively.

The phase-detuning relationship for an ABR-CPT interrogation scheme eliminating probe-induced shifts is given by a simple approximated expression for the Raman phase $\Phi(\delta)$ when $\Omega_{1,2} \ll \Gamma$ as [56]:

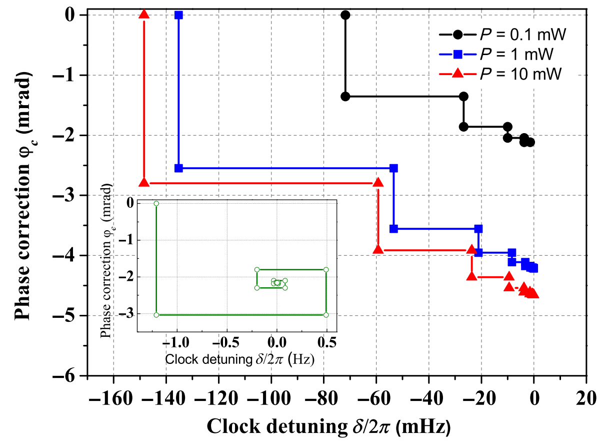

FIG. 1. Trajectory in the phase space after closing both servo loops. $T_1 = 5$ ms, $T_1/T_2 = 2.5$. Black dots, $P = 0.1$ mW; blue squares, $P = 1$ mW; red triangles, $P = 10$ mW. Inset: particular case, $T_1 = 0.5$ ms, $T_1/T_2 = 5$, $P = 0.1$ mW.

$$\Phi(\delta) \approx \arctan\left[\frac{\mathrm{Im}\{\rho_{12}\}}{\mathrm{Re}\{\rho_{12}\}}\right] = \frac{(\Delta_1 - \Delta_2) + \bar{\Delta}\gamma_c}{(\Delta_1 - \Delta_2)\bar{\Delta} - \gamma_{\mathrm{eff}}}, \qquad (2)$$

where ρ_{12} is the hyperfine coherence in the density matrix formalism. Other parameters γ_{eff} and $\bar{\Delta}$ are defined as

$$\gamma_{\mathrm{eff}} = \gamma_c + \frac{\Omega_1^2}{\gamma_2} + \frac{\Omega_2^2}{\gamma_1}, \qquad (3)$$

and

$$\bar{\Delta} = \frac{\Omega_2^2 \Gamma_{31} \gamma_2 \Delta_1 - \Omega_1^2 \Gamma_{32} \gamma_1 \Delta_2}{\gamma_1 \gamma_2 (\Omega_2^2 \Gamma_{31} + \Omega_1^2 \Gamma_{32})}. \qquad (4)$$

The set of equations given by Eq. (1) automatically converges after an iterative process to the set of the following stable parameters:

$$\delta(\varphi_c) = 0, \qquad \varphi_c = \Phi(\eta_1, \eta_2)|_{\delta=0}. \qquad (5)$$

An example of the system trajectory in the phase space (δ, φ_c) after closing both loops is shown in Fig. 1 for three laser powers and a ratio $T_1/T_2 = 2.5$. The starting points are different because the probe-induced shifts are different. A detuning $\delta = 0$, i.e., without frequency shift, is reached in only a few steps, demonstrating the method efficiency. It can be noted that in particular cases the trajectory can be different of a staircase shape, as seen in the inset of Fig. 1 where a spiral shape is observed for $T_1/T_2 = 5$ and $T_1 = 0.5$ ms. For this study, we used approximated experimental parameter values extracted from Ref. [13], including broadening effects on optical lines by buffer gas as follows:

$$
\begin{aligned}
\Gamma_{31} &= \Gamma_{32} \sim \Gamma/2 = 2\pi \times 200 \text{ MHz}, \\
\gamma_1 &= \gamma_2 = (\Gamma_{31} + \Gamma_{32})/2 \sim \Gamma/2, \\
\gamma_c &\sim 2\pi \times 400 \text{ Hz}, \\
\eta_1 - \eta_2 &\sim 2\pi \times 7.5 \times 10^{-12}\ \Omega^2 \text{ Hz}, \\
T_1 &\sim 5 \text{ ms}, \\
T_2 &\sim 2 \text{ ms}, \\
\Omega_1 &= \Omega_2 \sim 2 \times 10^6 \times \sqrt{P/S}, \qquad (6)
\end{aligned}
$$

where P is the light power and $S = 3 \times 10^{-4}$ m^2 is the beam area.

III. EXPERIMENTAL SETUP

Figure 2 describes the CPT-based Cs vapor-cell clock schematic. The latter, previously described in Ref. [13], combines an optimized CPT pumping scheme named push-pull optical pumping (PPOP) [58,59] and a pulsed interrogation scheme. The laser source is a distributed feedback (DFB) diode laser tuned on the Cs D_1 line at 894.6 nm. A 70-dB optical isolation stage is implemented at the output of the laser to prevent optical feedback. The laser light is injected into a temperature-stabilized fibered Mach-Zehnder intensity electro-optic modulator (MZ EOM). The latter is modulated at 4.596 GHz by a low phase noise microwave frequency synthesizer [60] in order to produce two highly coherent first-order optical sidebands that are frequency split by 9.192 GHz. At the output of the EOM, a dual-frequency sub-Doppler spectroscopy system in a pure Cs reference cell is implemented for stabilization of the laser frequency [61,62] onto the Cs $F' = 4$ excited state. The other fraction of the light is sent into an acousto-optic modulator (AOM) driven by a radio-frequency (rf) synthesizer in order to shift the laser frequency by −122 MHz and compensate for the buffer gas induced optical frequency shift in the CPT cell [63]. The signal from the AOM rf synthesizer driver can be switched on and off in order to produce the pulsed CPT interaction. The laser beam is then sent into a Michelson-like system allowing to produce the PPOP scheme [58,59], in which atoms interact with two bichromatic optical fields, exhibiting orthogonal circular polarizations and a half-clock period delay. This pumping scheme helps to generate the constructive interference of two successive dark states, yielding most of the atoms whatever their initial state to be pumped into the 0-0 clock transition. At the output of the Michelson system, a beam splitter is used to divide the laser beam into two sub-beams. The first sub-beam is detected by a low-noise photodiode associated with a homemade optical power servo system operating in the pulsed regime (see Sec. IV). The other sub-beam, expanded and collimated to a diameter of 2 cm, is sent towards a Cs vapor cell (2-cm diameter and 5-cm length) filled with a buffer gas mixture of nitrogen and argon (pressure ratio $r = P_{\text{Ar}}/P_{N_2} = 0.6$) of total pressure 15.3 Torr. The cell is temperature stabilized at 35 °C. A solenoid is used to generate a static magnetic field of 5 μT parallel to the laser beam, in order to make arise the Zeeman manifold. The cell ensemble is protected by a double-layer μ-metal magnetic shield. The laser beam at the output of the cell is focused using a converging lens and detected by a photodiode. The full clock operation is ensured using a multifunction data acquisition card piloted by a computer and a dedicated Python software.

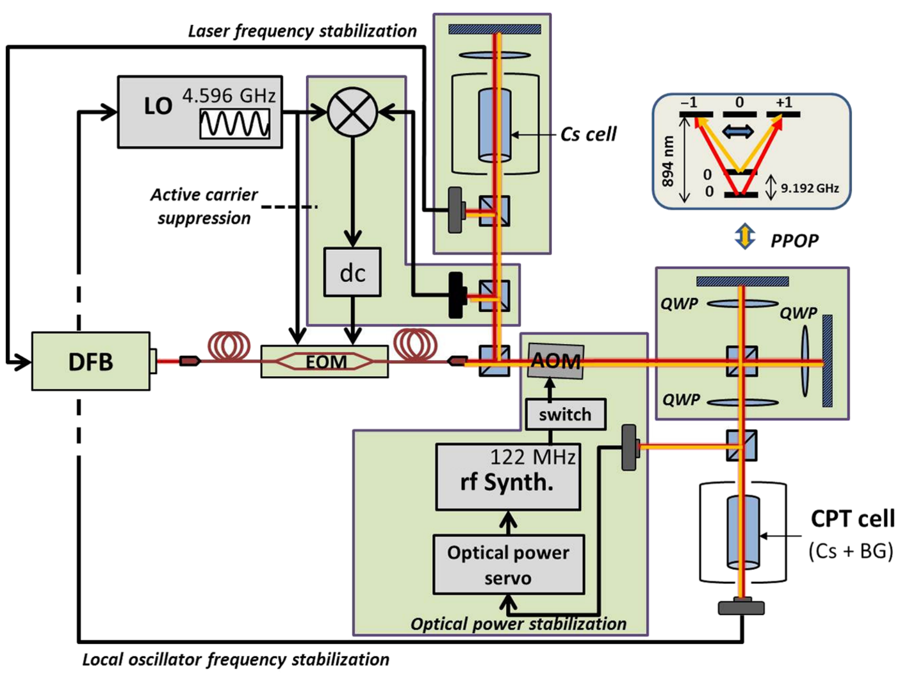

FIG. 2. Schematic of the CPT-based clock. DFB, distributed feedback laser; EOM, Mach-Zehnder electro-optic modulator; AOM, acousto-optic modulator; rf synth., radio-frequency synthesizer used to drive the AOM; switch, microwave switch used to produce the pulsed light sequence; LO, local oscillator; dc, dc bias voltage applied onto the MZ EOM; Cs + BG, buffer gas-filled Cs vapor-cell. The total optical-path length difference between both arms of the Michelson system is $\lambda_{\text{Cs}}/2 \sim 16.2$ mm where λ_{Cs} is the clock transition wavelength. The full clock operation, including the control of the 4.6-GHz synthesizer (phase and frequency), is ensured by a multifunction card (NI-USB6259) and a computer (not shown). The inset shows the push-pull optical pumping (PPOP) CPT-scheme diagram involved in the experiment.

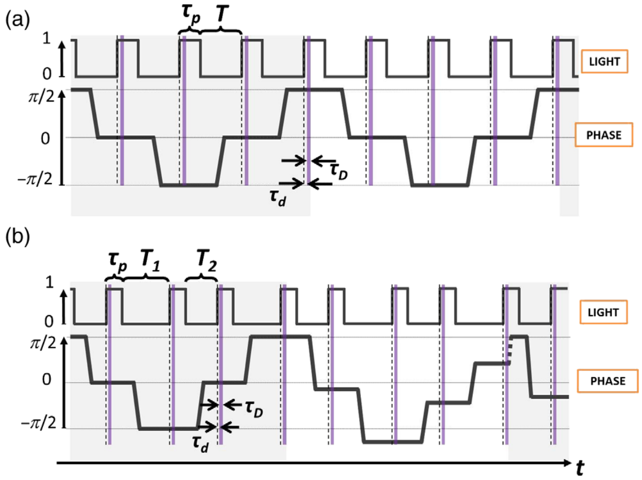

FIG. 3. Pulsed CPT sequence. (a) Ramsey-CPT (with phase modulation); (b) ABR-CPT. The atoms interact with the light during pulses of length τ_p, spaced apart by free-evolution times T, T_1, or T_2. Each pulse is the second pulse of the previous Ramsey interrogation and the first one of the next Ramsey interrogation. The signal is detected at the beginning of each pulse, after a delay time τ_d, and averaged during τ_D. The vertical dashed lines show the rising edges of the pulses, the solid vertical lines show the detection time. For more clarity, in (b), the phase sequence is shown without φ_c correction in the first shaded area, and with correction outside.

Figure 3 describes the Ramsey-CPT sequences performed in the usual Ramsey-CPT and ABR-CPT regimes, respectively.

In the Ramsey-CPT case, atoms interact with regular optical CPT pulses. The first CPT pulse pumps the atoms into the dark state using a typical duration τ_p of 1.1 ms. Atoms evolve then freely in the dark during a free-evolution time T of 2.7 ms before being detected at the next pulse, after a delay time τ_d of 20 μs during a detection window of duration τ_D of 80 μs. The clock signal is averaged over the detection window with a rate of 1 Msamples/s. The sequence cycle duration is noted $T_c = \tau_p + T$. The associated cycle frequency is noted $f_c = 1/T_c$. The output mean phase of the local oscillator (LO) is modulated at the frequency $f_m = 1/(4T_c)$. The phase is modified during the dark time. Smooth 50-μs ramp-based variations of the LO output phase are applied instead of pure square-wave phase modulation in order to avoid any LO-phase transient perturbations due to the LO-phase modulation. A $-\pi/2$ step is applied each first and second cycle of a period, and a $\pi/2$ step is applied each third and fourth cycle. The averaged CPT signal is synchronously demodulated in order to produce an error signal that zeroes when the LO frequency matches the CPT-resonance central frequency. A correction is applied to the LO frequency at the end of each period, just after the last detection window.

In the ABR-CPT method [see Fig. 3(b)], the sequence is based on the alternation of two successive Ramsey-CPT cycles with unequal free-evolution times $T_2 = 2.7$ ms and $T_1 = 5.4$ ms. The detection section is analog to the standard Ramsey-CPT case. The phase is twice decreased by $\pi/2$ in the middle of the first short and long dark times and increased twice again by $\pi/2$ in the middle of the following short and long dark times. An additional phase jump φ_c is applied at each $\pi/2$ phase transition. For each iteration, two error signals, one for dark times T_2 and T_1, are computed. The error signal extracted from the cycle with the short dark time T_2 is used to compute the value of the phase jump φ_c applied in the next iteration. The error signal extracted from the cycle with the long dark time T_1 is used to correct the LO frequency during the next iteration. As the mean phase of the 4.596 GHz synthesizer (see Ref. [60]) is incremented of $\varphi_c/2$ (i.e., φ_c on the 9-GHz signal) using a direct digital synthesizer (DDS) after each Ramsey-CPT pulse, the average DDS phase-modulation control voltage varies monotonically along time and eventually reaches its extreme value. In order to circumvent this issue and since only the phase step between two pulses is significant, the mean phase of the DDS is reset to zero (as sketched in Fig. 3 by the bold dashed line) immediately after the end of the last detection window of each ABR total period in order to compensate for the absolute phase drift. In both Ramsey-CPT and ABR-CPT cases, the clock output signal is counted by comparison with the signal of a reference active hydrogen maser [64].

IV. OPTICAL POWER STABILIZATION AND THERMAL ISOLATION

Enhanced thermal isolation of the experiment and laser-power stabilization have been firstly implemented in order to improve the clock-frequency stability performances.

The temperature fluctuations of the optical table are reduced using two passive polyurethane foam-based insulation boxes. The first box, being priorly the unique box to be used, covers the total top surface of the optical table. The second box, made of 10-cm-thick polyurethane foam, has been added in order to surround the whole experimental setup, including the first isolation box. The bottom surface of the second box is placed between the optical table breadboard bottom surface and the optical table legs in order to improve the setup thermal isolation from thermal fluxes coming from the ground and table legs. Figure 4 reports the typical temperature fluctuations of the laboratory room and of the experimental setup in respective cases where only the first box is used (past configuration) or where both boxes are implemented.

The laboratory room-temperature fluctuations are measured to be a few tens of mK for time scales up to 10 000 s. With the first isolation box, temperature fluctuations are reduced by a factor 2.6 and 6 at 5 s and 1000 s averaging time, respectively. The addition of the second isolation box allows a further reduction of the temperature fluctuations by a factor of 7.9 and 12 at 5 s and 100 s averaging time,

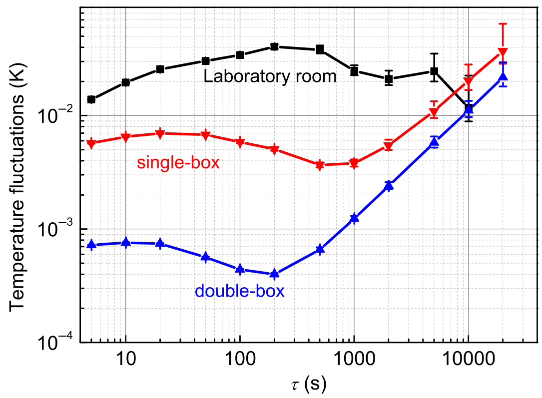

FIG. 4. Allan deviation of temperature fluctuations. All temperatures are measured using high-precision thermistors. The laboratory thermistor is arbitrarily suspended a few centimeters over the second box top surface.

respectively. For time scales higher than about 10^4 s, the thermal isolation of the optical setup is not significantly improved with the isolation boxes.

A laser-power servo loop dedicated to operate in the pulsed regime and described in Fig. 5 has been implemented at the output of the Michelson system.

Here, a small fraction of the laser power is extracted using a beam splitter and monitored by a photodiode to be converted into a dc analog voltage. This output voltage is compared using an ultra-low-noise instrumentation amplifier (AD8429, input voltage noise: 1 nV/$\sqrt{\mathrm{Hz}}$, voltage gain ∼100) to a digitally controlled high-resolution voltage set point extracted from a digital-to-analog converter (DAC AD5541) referenced to a low-drift reference voltage (LM399, 0.2 ppm/K). The output error signal is summed to an additional digitally controlled voltage generated by a second DAC referenced to the same LM399 reference voltage. This additional DAC allows, in closed-loop

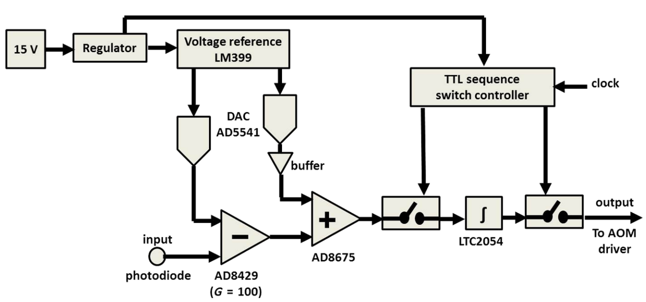

FIG. 5. Simplified schematic of the laser-power servo electronics. The photodiode detects an optical light pulse sequence, synchronized and trigged by the pulsed sequence applied onto the AOM. The laser-power electronics board reads the photodiode signal when the light is on, generates the error signal by comparison with the reference voltage, + and applies the correction to the laser power during the pulse. When the light is off, both switches must be opened rapidly with high isolation to prevent any undesired correction.

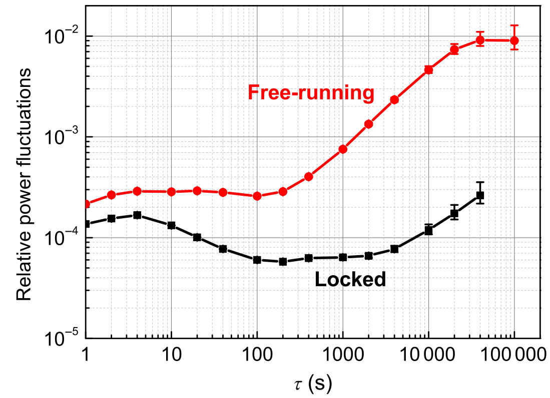

FIG. 6. Allan deviation of relative laser-power fluctuations in free-running and locked regimes.

operation, the tuning and control of the photodiode output voltage with a μV resolution. The error signal is processed into a PI controller, yielding a correction signal which is applied onto the AOM driving synthesizer rf power. The PI controller is inserted between two high-isolation and fast switches (ADG601, 60-dB isolation, switching time ∼50 ns), switched on and off synchronously with the pulsed Ramsey transistor-transistor logic (TTL) sequence. The laser-power monitoring and the application of the correction signal is performed on each light pulse with a servo bandwidth of about 2 kHz. Figure 6 plots the measured relative laser-power fluctuations at the input of the CPT cell in free-running and locked regimes. The fractional laser-power stability is improved by a factor 1.5 and 40 in the locked regime at 1 s and 10^4 s integration time, respectively.

V. FREQUENCY MEASUREMENTS

Figure 7 shows a typical Ramsey-CPT fringe detected in the Cs vapor cell for a total input laser power of 800 μW and a free-evolution time T of 2.7 ms. The central fringe linewidth is about 185 Hz. The fringe contrast C defined as

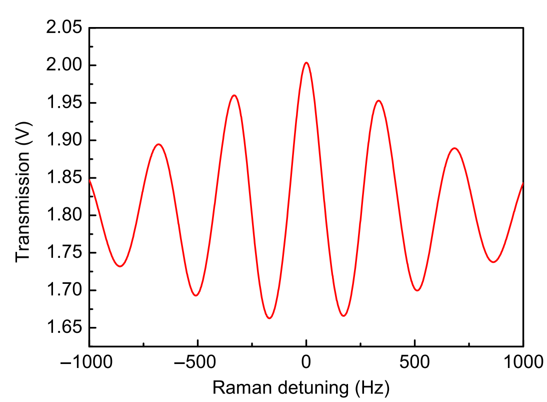

FIG. 7. Typical Ramsey-CPT fringe. The laser power is 800 μW and the free-evolution time T is 2.7 ms.

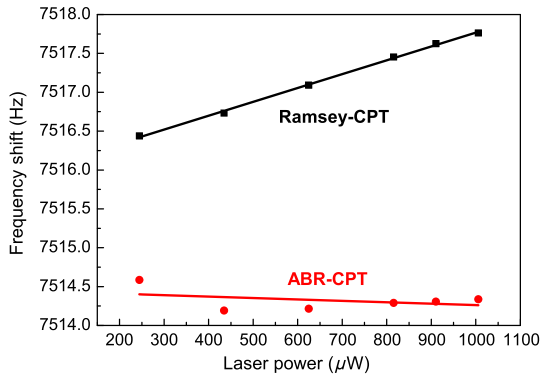

FIG. 8. Clock-frequency shift (offset from 9.192 631 770 GHz) versus the laser power in the Ramsey-CPT regime or the ABR-CPT protocol. Error bars are included in the size of the dots.

the fringe amplitude (0.35 V) divided by the fringe half-height dc level (1.835 V) is 19%.

Figure 8 reports the clock-frequency shift (offset from 9.192 631 770 GHz) versus the laser power in the Ramsey-CPT regime or using the ABR-CPT protocol. In the Ramsey-CPT case, experimental data are well fitted by a linear function in the studied power range. The light-shift coefficient is in fractional value about $2 \times 10^{-13}/\mu$W for $T_R = 2.7$ ms. For optical power lower than 200 μW, we observe that the frequency shift does not vary linearly with the laser power, as already observed in previous studies [20,44,65,66]. Using the ABR-CPT interrogation protocol, experimental data are here fitted by a linear function, yielding a sensitivity in fractional value of about $-2.5 \times 10^{-14}/\mu$W (with $T_2 = 2.7$ ms and $T_1 = 5.4$ ms), a factor 8 times lower than in the Ramsey-CPT case.

Figure 9 shows the trajectory of the real system in the phase space (φ_c, δ) after closing both interconnected phase and frequency servo loops of the ABR-CPT technique. The $\delta = 0$ value is defined as the steady-state value. The tadpolelike shape trajectory illustrates the case described in Fig. 1. Here, in experimental conditions, the staircase shape of the resonance is not visible because values of φ_c and δ are recorded only every ten iterations. For this reason, the initial phase is not null. A greater number of iterations is also necessary compared to the simplified model of Sec. II. This could be due to the warm-up time of the AOM generating the optical pulses, the presence of noise, and to the presence of other atomic levels. Here, in a real Cs experiment, optical transitions between 32 levels are involved instead of three in our simplified model. The inset of Fig. 9 shows an enlargement of the phase-frequency detuning diagram, when both interleaved loops have reached the steady state. The size of the final spot region represents typical phase and frequency fluctuations obtained in the steady-state regime, consistent with a short-term fractional frequency stability value of about 3×10^{-13} at 1 s.

Figure 10 reports the Allan deviation of the CPT clock using the Ramsey-CPT mode or the ABR-CPT interrogation protocol. In the Ramsey-CPT case, the short-term fractional frequency stability is improved by a factor of 1.6 compared to Ref. [13], yielding the level of $1.45 \times 10^{-13}\ \tau^{-1/2}$ up to 200 s. This stability improvement is attributed to the reduction of laser-power fluctuations thanks to the laser-power servo described in Sec. IV. Short-term stability performances are here comparable to best Rb-cell frequency standards [14,67]. The clock Allan deviation at 10^4 s averaging time is at the level of 10^{-13}, a factor of 10 better than in Ref. [13]. Here also, the improvement is attributed to improved laser-power stabilization. Moreover, contrary to the results shown in Ref. [13], the present Allan deviation plot exhibits a well-defined $1/\sqrt{\tau}$ slope, without any undesired bumps. This minor improvement could be attributed to the enhanced thermal isolation of the experiment.

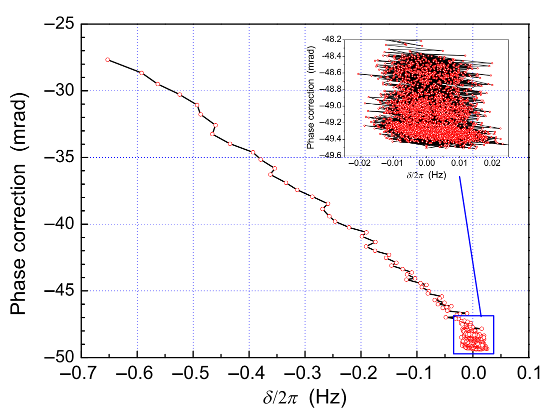

FIG. 9. Example of trajectory of the system in the phase space after closing the frequency and phase loops in the ABR technique. The laser-power incident in the cell is 800 μW. Free-evolution times are 2.7 and 5.4 ms. The solid line is a guide for the eye. $\delta = 0$ is defined as the steady-state value.

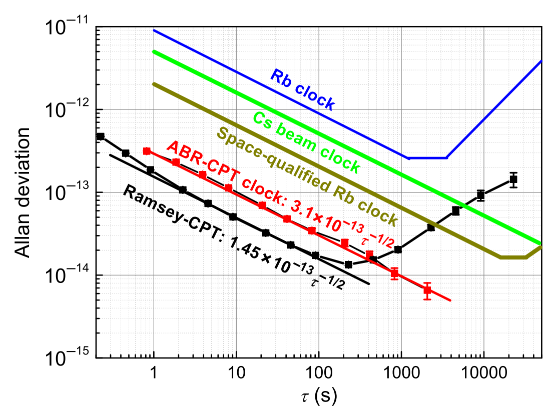

FIG. 10. Allan deviation of the CPT clock using the Ramsey-CPT or the ABR-CPT interrogation methods. The laser-power incident in the cell is 800 μW. For comparison, performances of a high-performance commercial Cs beam clock, Rb clock, and space-qualified Rb clocks (for GPS systems) [6] are reported.

Using the ABR-CPT protocol, the clock short-term frequency stability is degraded by a factor of 2, yielding 3.1×10^{-13} at 1 s. This degradation is in correct agreement with the reduction of the Ramsey-CPT fringe signal for $T = 5.4$ ms, compared to $T = 2.7$ ms, due to the relaxation of the CPT coherence [13]. Indeed, in this preliminary test, the error signal for the LO frequency correction is extracted from the cycle with long free-evolution time $T_1 = 5.4$ ms. Moreover, with the ABR-CPT protocol, the cycle time used for extracting the LO-phase correction signal acts as a dead time (loss of information) for the LO frequency servo loop. On the other hand, the Allan deviation of the clock is improved at the level of 6×10^{-15} at 2000 s averaging time using the ABR-CPT protocol. These performances represent an improvement by a factor of 6.6 compared to the Ramsey-CPT case, in correct agreement with the reduction of the clock-frequency sensitivity to laser power. Further tests will be performed in the future to evaluate the ABR-CPT clock-frequency stability on longer time scales, by evaluating the impact of some experimental parameters, optimizing the ABR-CPT sequence, or proposing the implementation of variants of the ABR-CPT sequence [68].

VI. CONCLUSIONS

We report a theoretical study and successful experimental implementation of the autobalanced Ramsey interrogation protocol to a pulsed Cs vapor-cell atomic clock based on coherent population trapping. This original approach allows a compensation of residual uncompensated light shifts induced by the probing laser field, combined with an efficient stabilization of the clock frequency. This method has been found to reduce the sensitivity of the clock frequency to laser-power variations. In addition, dedicated electronics have been developed to stabilize the laser power in the pulsed regime and the thermal isolation of the clock experiment has been considered with precaution. The Allan deviation of the ABR-CPT clock is $3.1 \times 10^{-13}\tau^{-1/2}$, averaging down to the level of 6×10^{-15} at 2000-s integration time. We believe that frequency stability performances of this clock could be improved further in the future by optimizing the ABR-CPT sequence or some of its variants [68] and implementing still-improved electronics. These results reveal exciting perspectives towards the development of high-stability CPT-based atomic-frequency standards exhibiting numerous potential scientific and industrial applications. The ABR protocol should be also of great interest to be applied in other kinds of compact atomic clocks such as cold-atom CPT clocks or pulsed optically pumped Rb frequency standards.

ACKNOWLEDGMENTS

This work has been partly funded by the EMRP program (IND55 Mclocks). The EMRP is jointly funded by the EMRP participating countries within EURAMET and the European Union. This work was partly supported by the Agence Nationale de la Recheche (ANR) through the Programme d'Investissement d'Avenir (PIA) under the Oscillator IMP project and the FIRST-TF network. The Oscillator IMP [69] has been certified as an Equipment of Excellence project (ANR-11-EQPX-0033-OSC IMP) by the French government. The FIRST-TF network [70] has been certified as a Labex, or a Laboratory of Excellence (ANR-10-LABX-48-01) by the French government. This work was also supported by Région Bourgogne Franche-Comté intended to support the PIA. G. C. received funding by Région Bourgogne Franche-Comté. M. P. is supported by the FIRST-TF network. The authors thank P. Abbé (FEMTO-ST) for technical support and help for the implementation of the second temperature insulation box. The authors acknowledge C. Calosso (INRIM) for fruitful and stimulating discussions.

[1] L. S. Cutler, Fifty years of commercial caesium clocks, Metrologia **42**, S90 (2005).

[2] https://www.microsemi.com/product-directory/cesium-frequency-references/4115-5071a-cesium-primary-frequency-standard.

[3] J. Camparo, The rubidium atomic clock and basic research, Phys. Today **60**, No. 11, 33 (2007).

[4] J. Vanier and C. Mandache, The passive optically pumped Rb standard: The laser approach, Appl. Phys. B **87**, 565 (2007).

[5] P. Rochat, F. Droz, P. Mossin, G. Barmaverain, Q. Wang, D. Boving, L. Mattioni, M. Belloni, M. Gioia, U. Schmidt, T. Pike, and F. Emma, The onboard Galileo rubidium and passive maser, status and performance, in *Proceedings of the European Frequency and Time Forum* (EFTF, Besançon, France, 2005), pp 26–32, http://www.eftf.org/previousMeetingDetail.php?year=2005.

[6] V. Formichella, J. Camparo, and P. Tavella, Influence of the ac-Stark shift on GPS atomic clock timekeeping, Appl. Phys. Lett. **110**, 043506 (2017).

[7] A. Godone, F. Levi, C. E. Calosso, S. Micalizio, and A. Godone, High-performing vapor-cell frequency standards, Riv. Nuovo Cimento **38**, 133 (2015).

[8] G. Alzetta, A. Gozzini, L. Moi, and G. Orriols, An experimental method for the observation of r.f. transitions and laser beat resonances in oriented Na vapour, Nuovo Cimento Soc. Ital. Fis. B **36**, 5 (1976).

[9] E. Arimondo, Coherent population trapping in laser spectroscopy, Prog. Opt. **35**, 257 (1996).

[10] J. M. Danet, M. Lours, S. Guérandel, and E. De Clercq, Dick effect in a pulsed atomic clock using coherent population trapping, IEEE Trans. Ultrason. Ferroelectr. Freq. Control **61**, 567 (2014).

[11] M. Abdel Hafiz and R. Boudot, A coherent population trapping Cs vapor cell atomic clock based on push-pull optical pumping, J. Appl. Phys. **118**, 124903 (2015).

[12] P. Yun, F. Tricot, C. E. Calosso, S. Micalizio, B. Francois, R. Boudot, S. Guérandel, and E. de Clercq, High-Performance

Coherent Population Trapping Clock with Polarization Modulation, Phys. Rev. Applied **7**, 014018 (2017).

[13] M. Abdel Hafiz, G. Coget, P. Yun, S. Guérandel, E. de Clercq, and R. Boudot, A high-performance Raman-Ramsey Cs vapor cell atomic clock, J. Appl. Phys. **121**, 104903 (2017).

[14] S. Micalizio, C. E. Calosso, A. Godone, and F. Levi, Metrological characterization of the pulsed Rb clock with optical detection, Metrologia **49**, 425 (2012).

[15] S. Kang, M. Gharavipour, C. Affolderbach, F. Gruet, and G. Mileti, Demonstration of a high-performance pulsed optically pumped Rb clock based on a compact magnetron-type microwave cavity, J. Appl. Phys. **117**, 104510 (2015).

[16] J. Vanier, M. W. Levine, S. Kendig, D. Janssen, C. Everson, and M. J. Delaney, Practical realization of a passive coherent population trapping frequency standard, IEEE Trans. Instrum. Meas. **54**, 2531 (2005).

[17] N. Castagna, R. Boudot, S. Guérandel, E. de Clercq, N. Dimarcq, and A. Clairon, Investigations on continuous and pulsed interrogation for a CPT atomic clock, IEEE Trans. Ultrason. Ferroelectr. Freq. Control **56**, 246 (2009).

[18] R. Boudot, S. Guérandel, E. de Clercq, N. Dimarcq, and A. Clairon, Current status of a pulsed CPT Cs cell clock, IEEE Trans. Instrum. Meas. **58**, 1217 (2009).

[19] O. Kozlova, E. de Clercq, and S. Guérandel, Temperature and pressure shift of the Cs clock transition in the presence of buffer gases: Ne, N_2, Ar, Phys. Rev. A **83**, 062714 (2011).

[20] O. Kozlova, J. M. Danet, S. Guérandel, and E. de Clercq, Limitations of long-term stability in a coherent population trapping Cs clock, IEEE Trans. Instrum. Meas. **63**, 1863 (2014).

[21] C. E. Calosso, A. Godone, F. Levi, and S. Micalizio, Enhanced temperature sensitivity in vapor-cell frequency standards, IEEE Trans. Ultrason. Ferroelectr. Freq. Control **59**, 2646 (2012).

[22] M. Zhu and L. S. Cutler, Theoretical and experimental study of light shift in a CPT-based Rb vapor cell frequency standard, in *Proceedings of the 32nd Annual Precise Time and Time Interval Systems and Applications Meeting, Reston, VA, 2000* (The Institute of Navigation, Manassas, VA, 2000), p. 311.

[23] F.-X. Esnault, E. Blanshan, E. N. Ivanov, R. E. Scholten, J. Kitching, and E. A. Donley, Cold-atom double-Λ coherent population trapping clock, Phys. Rev. A **88**, 042120 (2013).

[24] P. R. Hemmer, M. S. Shahriar, V. D. Natoli, and S. Ezekiel, AC Stark shifts in a two-zone Raman interaction, J. Opt. Soc. Am. B **6**, 1519 (1989).

[25] M. S. Shahriar, P. R. Hemmer, D. P. Katz, A. Lee, and M. G. Prentiss, Dark-state-based three-element vector model for the stimulated Raman interaction, Phys. Rev. A **55**, 2272 (1997).

[26] S. Knappe, Emerging topics: MEMS atomic clocks, in *Comprehensive Microsystems*, edited by Y. Gianchandani, O. Tabata, and H. Zappe (Elsevier, Netherlands, 2007).

[27] http://www.microsemi.com/products/timing-synchronization-systems/embedded-timing-solutions/components/sa-45s-chip-scale-atomic-clock.

[28] V. Shah, V. Gerginov, P. D. D. Schwindt, S. Knappe, L. Hollberg, and J. Kitching, Continuous light-shift correction in modulated coherent population trapping clocks, Appl. Phys. Lett. **89**, 151124 (2006).

[29] B. H. McGuyer, Y. Y. Jau, and W. Happer, Simple method of light-shift suppression in optical pumping systems, Appl. Phys. Lett. **94**, 251110 (2009).

[30] Y. Zhang, W. Yang, S. Zhang, and J. Zhao, Rubidium chip-scale atomic clock with improved long-term stability through light intensity optimization and compensation for laser frequency detuning, J. Opt. Soc. Am. B **33**, 1756 (2016).

[31] D. Miletic, C. Affolderbach, M. Hasegawa, R. Boudot, C. Gorecki, and G. Mileti, AC Stark-shift in CPT-based Cs miniature atomic clocks, Appl. Phys. B **109**, 89 (2012).

[32] N. F. Ramsey, A molecular beam resonance method with separated oscillating fields, Phys. Rev. **78**, 695 (1950).

[33] J. E. Thomas, P. R. Hemmer, S. Ezekiel, C. C. Leiby, R. H. Picard, and C. R. Willis, Observation of Ramsey Fringes Using a Stimulated, Resonance Raman Transition in a Sodium Atomic Beam, Phys. Rev. Lett. **48**, 867 (1982).

[34] P. R. Hemmer, S. Ezekiel, and J. C. C. Leiby, Stabilization of a microwave oscillator using a resonance Raman transition in a sodium beam, Opt. Lett. **8**, 440 (1983).

[35] T. Zanon, S. Guérandel, E. de Clercq, D. Holleville, N. Dimarcq, and A. Clairon, High Contrast Ramsey Fringes with Coherent-Population-Trapping Pulses in a Double Lambda Atomic System, Phys. Rev. Lett. **94**, 193002 (2005).

[36] S. Guérandel, T. Zanon, N. Castagna, F. Dahes, E. De Clercq, N. Dimarcq, and A. Clairon, Raman-Ramsey interaction for coherent population trapping Cs clock, IEEE Trans. Instrum. Meas. **56**, 383 (2007).

[37] G. S. Pati, K. Salit, R. Tripathi, and M. S. Shahriar, Demonstration of Raman-Ramsey fringes using time delayed optical pulses in rubidium vapor, Opt. Commun. **281**, 4676 (2008).

[38] P. Yun, Y. Zhang, G. Liu, W. Deng, L. You, and S. Gu, Multipulse Ramsey-CPT interference fringes for the 87 Rb clock transition, Europhys. Lett. **97**, 63004 (2012).

[39] I. Yoshida, N. Hayashi, K. Fujita, S. Taniguchi, Y. Hoshina, and M. Mitsunaga, Line-shape comparison of electromagnetically induced transparency and Raman Ramsey fringes in sodium vapor, Phys. Rev. A **87**, 023836 (2013).

[40] J. Yang, Y. Tian, B. Tan, P. Yun, and S. Gu, Exploring Ramsey-coherent population trapping atomic clock realized with pulsed microwave modulated laser, J. Appl. Phys. **115**, 093109 (2014).

[41] P. Yun, J. M. Danet, D. Holleville, E. de Clercq, and S. Guérandel, Constructive polarization modulation for coherent population trapping clock, Appl. Phys. Lett. **105**, 231106 (2014).

[42] X. L. Sun, J. W. Wang, P. F. Cheng, C. Xu, L. Zhao, and L. J. Wang, Investigation of Ramsey spectroscopy in a lin-par-lin Ramsey coherent population trapping clock with dispersion detection, Opt. Express **24**, 4532 (2016).

[43] E. Kuchina, E. E. Mikhailov, and I. Novikova, Effect of atomic diffusion on the Raman-Ramsey coherent population trapping resonances, J. Opt. Soc. Am. B **33**, 610 (2016).

[44] E. Blanshan, S. M. Rochester, E. Donley, and J. Kitching, Light shifts in a pulsed cold-atom coherent-population-trapping clock, Phys. Rev. A **91**, 041401(R) (2015).

[45] X. Liu, E. Ivanov, V. I. Yudin, J. Kitching, and E. A. Donley, Low-Drift Coherent Population Trapping Clock Based on Laser-Cooled Atoms and High-Coherence Excitation Fields, Phys. Rev. Applied **8**, 054001 (2017).

[46] X. Liu, V. I. Yudin, A. Taichenachev, J. Kitching, and E. A. Donley, High contrast dark resonances in a cold-atom clock probed with counterpropagating circularly polarized beams, Appl. Phys. Lett. **111**, 224102 (2017).

[47] A. Taichenachev, V. Yudin, C. Oates, Z. Barber, N. Lemke, A. Ludlow, U. Sterr, C. Lisdat, and F. Riehle, Compensation of field-induced frequency shifts in Ramsey spectroscopy of optical clock transitions, JETP Lett. **90**, 713 (2010).

[48] V. I. Yudin, A. V. Taichenachev, C. W. Oates, Z. W. Barber, N. D. Lemke, A. D. Ludlow, U. Sterr, Ch. Lisdat, and F. Riehle, Hyper-Ramsey spectroscopy of optical clock transitions, Phys. Rev. A **82**, 011804(R) (2010).

[49] N. Huntemann, B. Lipphardt, M. Okhapkin, Chr. Tamm, E. Peik, A. V. Taichenachev, and V. I. Yudin, Generalized Ramsey Excitation Scheme with Suppressed Light Shift, Phys. Rev. Lett. **109**, 213002 (2012).

[50] R. Hobson, W. Bowden, S. A. King, P. E. G. Baird, I. R. Hill, and P. Gill, Modified hyper-Ramsey methods for the elimination of probe shifts in optical clocks, Phys. Rev. A **93**, 010501(R) (2016).

[51] T. Zanon-Willette, E. de Clercq, and E. Arimondo, Probe light-shift elimination in generalized hyper-Ramsey quantum clocks, Phys. Rev. A **93**, 042506 (2016).

[52] V. I. Yudin, A. V. Taichenachev, M. V. Okhapkin, S. N. Bagayev, Chr. Tamm, E. Peik, N. Huntemann, T. E. Mehlstaubler, and F. Riehle, Atomic Clocks with Suppressed Blackbody Radiation Shift, Phys. Rev. Lett. **107**, 030801 (2011).

[53] V. I. Yudin, A. V. Taichenachev and M. Yu. Basalaev and T. Zanon-Willette, Synthetic frequency protocol for Ramsey spectroscopy of clock transitions, Phys. Rev. A **94**, 052505 (2016).

[54] T. Zanon-Willette, R. Lefevre, A. V. Taichenachev, and V. I. Yudin, Universal interrogation protocol with zero probe-field-induced frequency shift for quantum clocks and high-accuracy spectroscopy, Phys. Rev. A **96**, 023408 (2017).

[55] C. Sanner, N. Huntemann, R. Lange, C. Tann, and E. Peik, Auto-Balanced Ramsey Spectroscopy, Phys. Rev. Lett. **120**, 053602 (2018).

[56] T. Zanon-Willette, E. de Clercq, and E. Arimondo, Ultrahigh-resolution spectroscopy with atomic or molecular dark resonances: Exact steady-state line shapes and asymptotic profiles in the adiabatic pulsed regime, Phys. Rev. A **84**, 062502 (2011).

[57] T. Zanon-Willette, Etudes de transitions atomiques permises et interdites par spectroscopie laser en vue d'une application aux horloges optiques, Habilitation à diriger des Recherches, UPMC, Paris, https://tel.archives-ouvertes.fr/tel-00958399v2/document (2014).

[58] Y. Y. Jau, E. Miron, A. B. Post, N. N. Kuzma, and W. Happer, Push-Pull Optical Pumping of Pure Superposition States, Phys. Rev. Lett. **93**, 160802 (2004).

[59] X. Liu, J. M. Mérolla, S. Guérandel, C. Gorecki, E. de Clercq, and R. Boudot, Coherent population trapping resonances in buffer gas-filled Cs vapor cells with push-pull optical pumping, Phys. Rev. A **87**, 013416 (2013).

[60] B. François, C. E. Calosso, J. M. Danet, and R. Boudot, A low phase noise microwave frequency synthesis for a high-performance cesium vapor cell atomic clock, Rev. Sci. Instrum. **85**, 094709 (2014).

[61] M. Abdel Hafiz, G. Coget, E. De Clercq, and R. Boudot, Doppler-free spectroscopy on the Cs D_1 line with a dual-frequency laser, Opt. Lett. **41**, 13, 2982 (2016).

[62] M. Abdel Hafiz, D. Brazhnikov, G. Coget, A. Taichenachev, V. Yudin, E. de Clercq, and R. Boudot, High-contrast sub-Doppler absorption spikes in a hot atomic vapor cell exposed to a dual-frequency laser field, New J. Phys. **19**, 073028 (2017).

[63] G. A. Pitz, D. E. Wertepny, and G. P. Perram, Pressure broadening and shift of the cesium D_1 transition by the noble gases and N_2, H_2, HD, D_2, CH_4, C_2H_6, CF_4, and ^3He, Phys. Rev. A **80**, 062718 (2009).

[64] https://www.t4science.com/products/imaser3000/ (iMaser-ST 3000 specifications).

[65] Y. Yano, W. J. Gao, S. Goka, and M. Kajita, Theoretical and experimental investigation of the light shift in Ramsey coherent population trapping, Phys. Rev. A **90**, 013826 (2014).

[66] G. S. Pati, Z. Warren, N. Yu, and M. S. Shahriar, Computational studies of light shift in a Raman-Ramsey interference-based atomic clock, J. Opt. Soc. Am. B **32**, 388 (2015).

[67] T. Bandi, C. Affolderbach, C. Stefanucci, F. Merli, A. Skrivervik, and G. Mileti, Compact high-performance continuous-wave double-resonance rubidium standard with $1.4 \times 10^{-13}\ \tau^{-1/2}$ stability, IEEE Trans. Ultrason. Ferroelectr. Freq. Control **61**, 1769 (2014).

[68] V. Yudin, A. V. Taichenachev, M. Yu. Basalaev, T. Zanon-Willette, J. W. Pollock, M. Shuker, E. A. Donley, and J. Kitching, Generalized Auto-balanced Ramsey Spectroscopy of Clock Transitions, Phys. Rev. Applied **9**, 054034 (2018).

[69] http://oscillator-imp.com/dokuwiki/doku.php.

[70] http://first-tf.com/.